Temporal compartmentalization of viral infection in bacterial cells

Audrey Labarde[a], Lina Jakutyte[b,1], Cyrille Billaudeau[c,1], Beatrix Fauler[d], Maria López-Sanz[e], Prishila Ponien[f], Eric Jacquet[f], Thorsten Mielke[d], Silvia Ayora[e], Rut Carballido-López[c], and Paulo Tavares[a,2]

[a]Université Paris-Saclay, CEA, CNRS, Institute for Integrative Biology of the Cell (I2BC), 91198 Gif-sur-Yvette, France; [b]Laboratoire de Virologie Moléculaire et Structurale, CNRS Unité Propre de Recherche 3296 and Institut Fédératif de Recherche 115, 91198 Gif-sur-Yvette, France; [c]Micalis Institute, INRAE, AgroParisTech, Université Paris-Saclay, 78350 Jouy-en-Josas, France; [d]Microscopy and Cryo-electron Microscopy Service Group, Max Planck Institute for Molecular Genetics, Ihnestrasse 63-73, 14195, Berlin, Germany; [e]Department of Microbial Biotechnology, Centro Nacional de Biotecnología, Consejo Superior de Investigaciones Científicas, 28049 Madrid, Spain; and [f]Université Paris-Saclay, CNRS, Institut de Chimie des Substances Naturelles, UPR 2301, 91198, Gif-sur-Yvette, France

Edited by Sankar Adhya, National Institutes of Health, National Cancer Institute, Bethesda, MD, and approved April 9, 2021 (received for review August 30, 2020)

Virus infection causes major rearrangements in the subcellular architecture of eukaryotes, but its impact in prokaryotic cells was much less characterized. Here, we show that infection of the bacterium *Bacillus subtilis* by bacteriophage SPP1 leads to a hijacking of host replication proteins to assemble hybrid viral–bacterial replisomes for SPP1 genome replication. Their biosynthetic activity doubles the cell total DNA content within 15 min. Replisomes operate at several independent locations within a single viral DNA focus positioned asymmetrically in the cell. This large nucleoprotein complex is a self-contained compartment whose boundaries are delimited neither by a membrane nor by a protein cage. Later during infection, SPP1 procapsids localize at the periphery of the viral DNA compartment for genome packaging. The resulting DNA-filled capsids do not remain associated to the DNA transactions compartment. They bind to phage tails to build infectious particles that are stored in warehouse compartments spatially independent from the viral DNA. Free SPP1 structural proteins are recruited to the dynamic phage-induced compartments following an order that recapitulates the viral particle assembly pathway. These findings show that bacteriophages restructure the crowded host cytoplasm to confine at different cellular locations the sequential processes that are essential for their multiplication.

bacteriophage | virus infection | phage DNA replication | virus assembly | bacterial cell compartmentalization

The organization of the cellular space is a common feature of living systems. Cell compartments delimited by membranes were observed in eukaryotic cells at the dawn of cell biology. More recently, membraneless self-organizing compartments were identified, adding further spatial order to the cell. Bacterial cells mainly rely on the latter type of strategy to structure their "open space" cytoplasm because they rarely feature intracellular membranes (1), although some notable exceptions exist (2). One well-documented case of membrane-free compartmentalization is the self-assembly of protein cages that confine biochemical reactions (3) or store specific cargo (4) in the bacterial cytoplasm. Considering their increasing variety, cell compartments are collectively defined here as a self-contained space that concentrates a set of macromolecular components inside the cell. Their boundaries can be established by membranes, a protein cage, or by the physicochemical properties of their components.

Lytic viral infection disrupts host cell homeostasis, reallocating extensive resources for virus multiplication. In eukaryotic viruses, this takeover correlates with the formation of virus replication compartments either in the host cytoplasm or in the nucleus (5). These viral factories can be membrane-associated structures as in case of several RNA virus families (6), membraneless viral DNA replication compartments (5), or liquid compartments formed by phase separation (7). The restructuration of bacterial cell architecture upon infection by bacterial viruses (phages or bacteriophages) is much less documented. DNA replication has been reported to occur at particular positions of the bacterial cytoplasm for four *Caudovirales*, a widely distributed order of double-stranded DNA viruses also known as tailed bacteriophages. Phage ϕ29 uses the actin-like MreB cytoskeleton and the bacterial nucleoid to position the protein-primed replication of its ∼20 kilo-base pair (kbp) genome at the periphery of the host cytoplasm (8, 9). Jumbo phages compartmentalize replication and transcription of their >200 kbp genome inside a viral proteinaceous nucleus-like cage that is positioned at midcell by a tubulin-related spindle (10–12). These are rare cases within the tailed phagosphere because of their particular mode of protein-primed replication (ϕ29) and of their genome size (ϕ29 and jumbo phages). The genomes of sequenced tailed phages have a median length of 51 kbp and those of the *Siphoviridae* family, which accounts for more than 55% of *Caudovirales*, are 48-kbp long on median (13). λ and SPP1, which typify the siphoviruses, accumulate their replicated DNA in a defined focus localized asymmetrically in the cell during lytic infection (14, 15), but further investigation is critical to assess the impact of their infection on cell biology.

Significance

Virus lytic infection disrupts host cell homeostasis and takes over the cell space for virus multiplication. Viral-induced reorganization of prokaryotic cells must meet the challenge to restructure the cytoplasm open space of a small-sized cell. We discovered that the bacterial siphovirus SPP1 builds two types of independent compartments in the host cytoplasm to confine viral DNA enzymatic reactions and to store viral particles. This spatial partition responds to the requirements for exponential replication of SPP1 genomes and for the assembly of hundreds of viral particles. Its similarities to remodeling of the cell nucleus by herpesviruses led to the hypothesis that ancestral strategies used by viruses to invade the cell space were conserved to infect hosts of different domains of life.

Author contributions: A.L., L.J., C.B., B.F., M.L.-S., P.P., E.J., T.M., S.A., R.C.-L., and P.T. designed research; A.L., L.J., C.B., B.F., M.L.-S., P.P., E.J., and P.T. performed research; A.L., L.J., C.B., M.L.-S., and P.T. contributed new reagents/analytic tools; A.L., L.J., C.B., B.F., M.L.-S., P.P., E.J., T.M., S.A., R.C.-L., and P.T. analyzed data; and A.L., S.A., R.C.-L., and P.T. wrote the paper.

The authors declare no competing interest.

This article is a PNAS Direct Submission.

[1]L.J. and C.B. contributed equally to this work.

[2]To whom correspondence may be addressed. Email: Paulo.Tavares@I2bc.Paris-Saclay.Fr.

This article contains supporting information online at https://www.pnas.org/lookup/suppl/doi:10.1073/pnas.2018297118/-/DCSupplemental.

Published July 9, 2021.

Here, we investigate cell host takeover by the well-characterized bacteriophage SPP1 (16–20), which infects the gram-positive model bacterium *Bacillus subtilis* (Fig. 1*A*). We discovered that phage infection leads to an extensive reorganization of the *B. subtilis* cytoplasmic space. SPP1 is shown to assemble two temporally and spatially independent types of compartments in the bacterial cytoplasm. A single compartment harbors viral genome replication and packaging, while the others are storage regions of viral particles (or virions).

Results

DNA Biosynthetic Challenge Imposed by Bacteriophage SPP1 Infection to the Host Cell. Genome replication and virion assembly are the key steps of virus multiplication (Fig. 1*A*) accounting

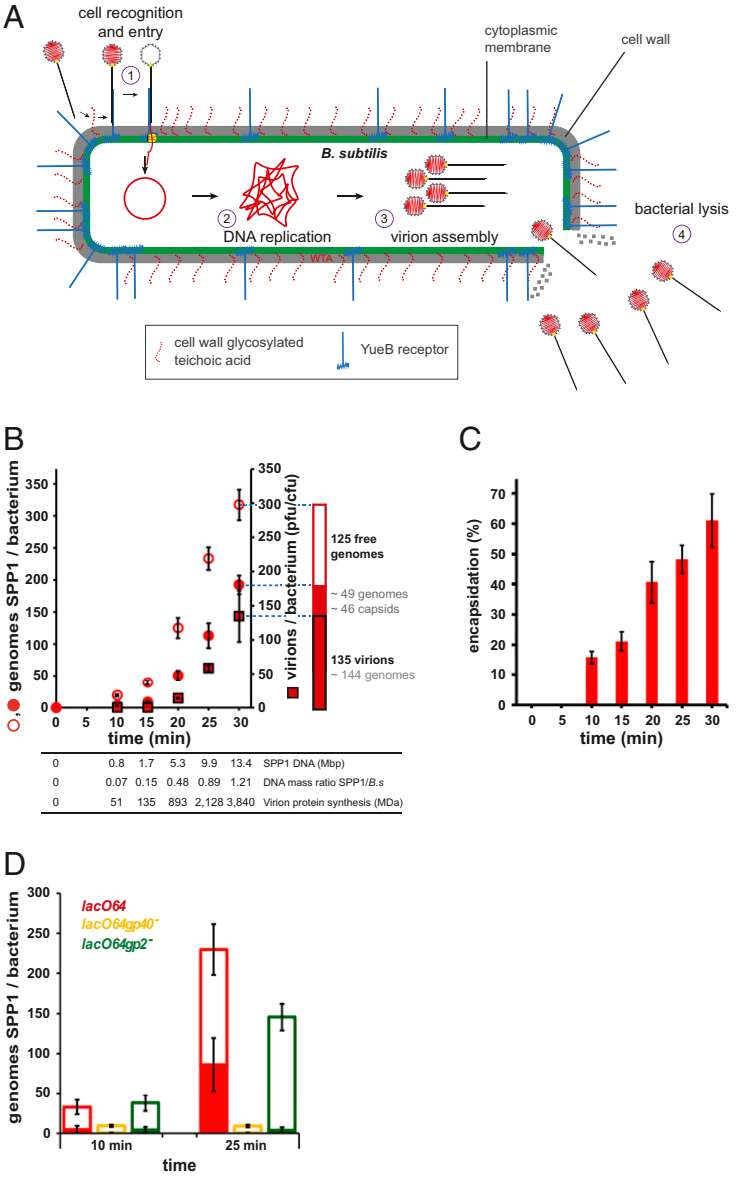

Fig. 1. SPP1 DNA replication and encapsidation. (*A*) Schematics of the main steps of tailed bacteriophage infection exemplified by SPP1. (*B*) Quantification of SPP1 DNA synthesis (empty circles) and encapsidation (filled circles) determined by qPCR of total and DNase-protected DNA, respectively, in *B. subtilis* GSY10004 infected with SPP1*lacO64*. The amount of SPP1 gene *6* DNA was divided by the amount of *B. subtilis gyrA* reporter DNA considering that there are 2.7 nucleoids on average per cell (*SI Appendix*, Fig. S1 *C* and *D*) to calculate the number of SPP1 genomes per bacterium. The total number of infectious particles (filled squares; ordinate on the right) was quantified by phage titration of bacteria lysed with 10% chloroform. Note that the DNA molecule encapsidated in SPP1*lacO64* particles (~45.1 kbp) is 1.07-fold longer than the phage genome size (42.3 kbp) (15, 66), a factor that was used to convert phage particle counts into genome equivalents and reciprocally. (*Right*) A snapshot of phage DNA and particle yields at 30 min p.i., when experiments were stopped because cell lysis initiated. The values in bold were obtained experimentally, and those in gray were calculated based on the figure data. Note that the calculation of ~46 capsids corresponds to particles that protect viral DNA but are noninfectious (i.e., tailless DNA-filled capsids and eventually defective tailed phage particles). The data are the average from three independent experiments. The biosynthetic effort accounting for phage DNA and virion structural proteins synthesis is depicted underneath the infection time points (Dataset S1). (*C*) Percentage of encapsidated DNA calculated from the data in *B*. (*D*) Phage DNA synthesis at 10 and 25 min p.i. in *B. subtilis* GSY10004 infected with SPP1*lacO64* (15) (red), SPP1*lacO64gp40*$^{-}$ (defective in initiation of DNA synthesis) (yellow), and SPP1*lacO64gp2*$^{-}$ (defective in DNA packaging) (green). Total DNA (bars total height) and encapsidated, DNase-protected DNA (overlapping full bars) were quantified by qPCR. The data are the average from three independent experiments.

for most of phage infection biosynthetic costs. To investigate their impact on the architecture of infected cells, we used a phage that carries an array of ∼64 *lacO* operator sites inserted in its genome (SPP1*delX110lacO64*). By infecting *B. subtilis* cells producing the cognate LacI-binding protein fused to a fluorescent protein (FP), phage DNA can be visualized during infection (15). SPP1*delX110lacO64* produces approximately two- to threefold less progeny virions than SPP1 wild type but impacts neither the phage temporal infection program nor the timing of phage lysis (*SI Appendix*, Fig. S1*A*) (15, 16). SPP1*delX110lacO64*, abbreviated SPP1*lacO64* from hereafter, and the *B. subtilis* strain producing LacI-mCherry are the parental viral and bacterial strains, respectively, used throughout the present study unless stated otherwise.

The DNA mass in SPP1*lacO64*-infected cells rose sharply after 15 min postinfection (p.i.) (*SI Appendix*, Fig. S1*B*). At 30 min p.i., when lysis initiates in rich medium cultures grown at 37 °C, total DNA increased approximately twofold relative to noninfected cells. The mean cell surface did not vary significantly during infection (2.71 ± 0.78 μm^2 ($n = 2{,}464$) in infected cells versus 2.85 ± 0.79 μm^2 ($n = 1{,}160$) in noninfected cells), indicating that the DNA/cytoplasmic space ratio was doubled. We next quantified bacterial and viral DNA during infection by qPCR. Viral genome replication was detectable at 10 min p.i. and increased exponentially until 30 min p.i. (Fig. 1*B*). At this stage of infection, each bacterium contained an average of 318 copies of the phage genome (Fig. 1*B*, empty circles) accounting for 13.4 mega base pairs (Mbp) of viral DNA, which exceeds the ∼11 Mbp of bacterial DNA present in the cell [equivalent to 2.7 copies of the 4.06 Mbp *B. subtilis* YB886 genome (*SI Appendix*, Fig. S1 *C* and *D*) (21)].

Genome encapsidation quantified by qPCR of deoxyribonuclease (DNase)-protected DNA was detected at 20 min p.i. (Fig. 1*B*, filled circles) due to its temporal delay relative to DNA replication (16). Only a fraction of the SPP1 DNA synthesized (reaching ∼60% at 30 min p.i.) was encapsidated inside viral particles (Fig. 1*B*, filled circles and Fig. 1*C*). The majority of those particles (∼75% at 30 min p.i.) were infectious as quantified in a phage titration plaque assay (Fig. 1*B*, squares). The noninfectious viral particles were likely DNA-filled capsids that did not yet attach tails in their assembly pathway (22) and possibly some defective tailed phage particles. Interestingly, SPP1 DNA synthesis was reduced in infections with a phage defective in the DNA packaging enzyme gp2 [SPP1*delX110lacO64sus19* (*SI Appendix*, Table S1) (23), hereafter abbreviated as SPP1*lacO64gp2*$^-$] that does not encapsidate DNA (Fig. 1*D*), indicating a regulatory feedback between genome encapsidation and DNA replication.

***B. subtilis* Replisome Proteins Are Recruited into Hybrid Phage–Host Replisomes at the Viral DNA Compartment.** Monoinfected *B. subtilis* cells display a single phage DNA focus (*SI Appendix*, Fig. S2 *A* and *B*), hereinafter referred to as the viral DNA compartment, which increases in size during infection (*SI Appendix*, Fig. S2*B*) (15). Since SPP1 requires several host proteins for the replication of its genome (*SI Appendix*, Table S2) (24–26), we investigated the subcellular localization of both SPP1 DNA and FP fusions to *B. subtilis* replisome components (Fig. 2*A* and *SI Appendix*, Fig. S2*C*). In noninfected bacteria, the DNA polymerase PolC, the clamp loader subunit DnaX, the sliding clamp DnaN, and the single-stranded DNA-binding protein SsbA localized into small foci, presumably the *B. subtilis* replisomes assembled at replication forks (arrowheads in Fig. 2*A* and *SI Appendix*, Fig. S2*C*) (27). Foci of the primosome protein DnaB and of the DNA polymerase DnaE were also detected in some cells, while the primase DnaG displayed a diffuse distribution (*SI Appendix*, Fig. S2 *C*, *Left*) (27, 28). Interestingly, in infected bacteria, all seven host proteins colocalized with SPP1 DNA, irrespectively of being essential (PolC, DnaE, DnaX, DnaN, and DnaG) or dispensable (SsbA and DnaB) for SPP1 multiplication (Fig. 2 and *SI Appendix*, Fig. S2*C* and Table S2). The colocalization of DnaE and DnaB FP fusions with phage DNA was more prominent early p.i., while the other host replisome components associated persistently to phage DNA during infection. Small foci of SsbA and more rarely of DnaX were also detected outside the viral DNA compartment in some infected cells (arrows in Fig. 2*A* and *SI Appendix*, Fig. S2*C*) possibly associated to host DNA. The *B. subtilis* replicative helicase DnaC showed a homogeneous distribution both in noninfected and infected bacteria (Fig. 2*B* and *SI Appendix*, Fig. S2*C*).

SPP1 infection led to a loss of the regular distribution of bacterial DNA replication origins in the cell (*SI Appendix*, Fig. S1*E*), but replication of the *B. subtilis* genome continued at least early during phage infection (*SI Appendix*, Fig. S1*F*). Nevertheless, the prominent spatial concentration of bacterial DNA replication effectors in the SPP1 DNA compartment correlated with a strong viral genome replication activity (Fig. 1*B* and *SI Appendix*, Fig. S1*G*) that outperforms DNA replication in the bacterial nucleoid (Fig. 1*B*). We concluded that the DNA replication machinery of *B. subtilis* is biochemically and spatially reprogrammed for SPP1 genome replication.

We next investigated how the host replisome is recruited to the phage DNA compartment in three-color imaging experiments in which SPP1 DNA, *B. subtilis* replication proteins, and SPP1 replication proteins were simultaneously labeled. SPP1 DNA replication is initiated by gp38 binding and the melting of the phage origins of replication (29). Then, gp39 loads the helicase gp40 to the open origins (26, 30). Gp40 is known to interact with the host clamp loader subunits DnaX (31) and with the primase DnaG (32, 33). The finding that a gp40-mCitrine fusion produced in noninfected *B. subtilis* displayed a replisome-like localization and colocalized with mCFP-DnaX (Fig. 3*A*) is consistent with those previously identified interactions. Thus, the SPP1 helicase is recruited to the *B. subtilis* replisome in the absence of other phage proteins. In infected cells, both gp40 and DnaX relocalized into two or more foci inside the SPP1 DNA compartment (Fig. 3*B*) as also observed for other host replisome components (Fig. 2*A* and *SI Appendix*, Fig. S2*C*). These results indicate that viral DNA replication factories composed of hybrid phage–host replisomes assemble at distinct positions within the viral DNA compartment.

Upon entry into the host cell, the SPP1 genome is circularized and undergoes several cycles of circle-to-circle (theta) replication, leading to an exponential increase of phage DNA template molecules, and then switches to a linear sigma replication mode to generate genome concatemers (Fig. 3*E*). The gp40 helicase is essential for SPP1 DNA synthesis in both modes (25, 26), providing a hallmark for localization of SPP1 replication throughout infection (Fig. 3*F*). The SPP1 recombinase gp35 is essential for the theta-to-sigma replication mode switch and the 5′-3′ exonuclease gp34.1 is the other major phage effector of this step (17, 34). We were unable to determine the subcellular localization of gp35 due to the aggregation of different FP fusions to gp35, but we obtained a functional gp34.1-mCitrine fusion. Gp34.1-mCitrine formed a small focus that increased in size and colocalized with phage DNA in infections with a SPP1 mutant defective for production of gp34.1 (Fig. 3*G*). Thus, the complete sequential program of SPP1 replication is compartmentalized in the phage DNA compartment.

Viral DNA Occupies a Self-Contained Dynamic Compartment. The presence of a single viral DNA compartment in monoinfected bacteria indicates that replication of the SPP1 DNA molecule, which entered the cell at the beginning of infection (Fig. 1*A*), occurs at a specific location in the cytoplasm where descendent viral genomes accumulate throughout infection (*SI Appendix*, Fig. S2 *A* and *B*). We then analyzed quantitatively this compartment position and shape in hundreds of monoinfected cells. The compartment grew as infection proceeded (Fig. 4*A*) and had a center of mass at about 1.2 μm from the cell proximal pole regardless its size (Fig. 4*B*). The cell diameter of *B. subtilis* (∼1 μm) rapidly

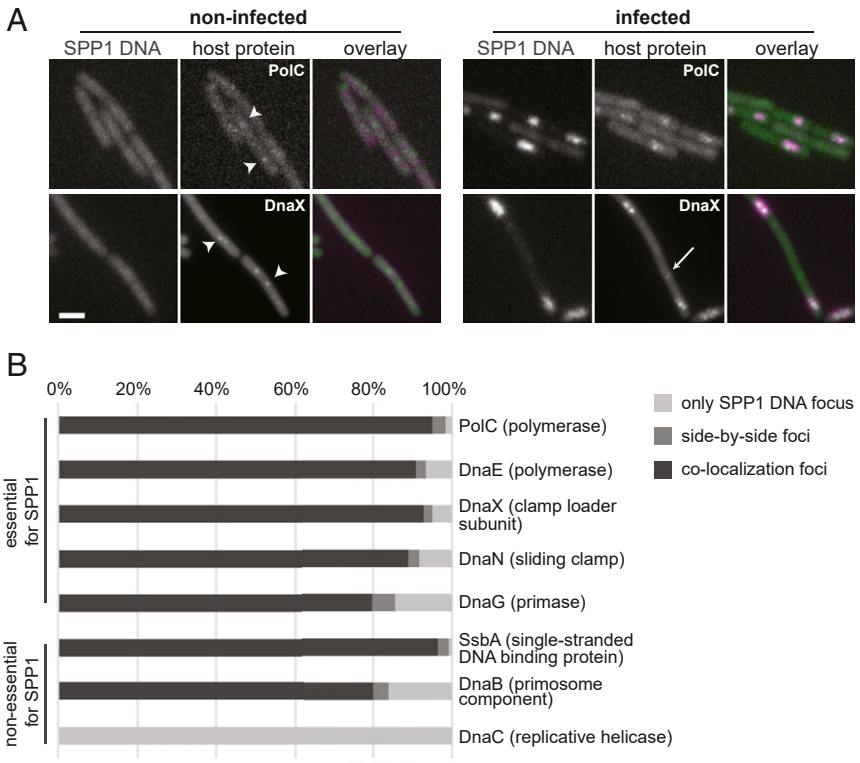

Fig. 2. Cellular localization of *B. subtilis* replisome proteins during SPP1 infection. (*A*) PolC-GFP (*Top*) and mCFP-DnaX (*Bottom*) in bacteria noninfected (*Left*) and infected with SPP1*lacO64* (*Right*) late p.i. (see *SI Appendix*, Fig. S2*B* for experimental setup). The *B. subtilis* strains produce LacI-mCherry constitutively. The signals on the RFP channel are displayed in magenta, while signals on GFP and CFP channels are in green on overlays, respectively. (Scale bar, 2 μm.) The arrowheads show the position of host replication protein foci in noninfected bacteria, and the arrow identifies a focus of mCFP-DnaX that does not colocalize with SPP1 DNA in an infected bacterium. (*B*) Quantitative analysis of *B. subtilis* replisome proteins localization relative to the SPP1 DNA focus in bacteria early p.i. according to the gray scale legend on the right. More than 100 cell counts were made for each strain.

constrained radial growth of the compartment leading to an elongated shape. Its area increased by longitudinal growth as DNA synthesis ensued (Fig. 4 *C*–*E*). Phage DNA accessible for LacI-mCherry labeling occupied, on average, 25% of the cell area late in infection (Fig. 4*A*, blue). This accounted only for ∼40% of the total SPP1 DNA synthesized because the remaining DNA shielded inside viral particles (Fig. 1 *B* and *C*) was stripped off of LacI-mCherry during its packaging into phage procapsids through a 30-Å wide portal channel. To visualize the total SPP1 DNA synthesized, we infected cells with SPP1*lacO64gp2*$^{-}$ that is defective in DNA packaging. In the absence of genome encapsidation, the viral DNA compartment grew into a significantly more elongated shape (Fig. 4 *C*–*E*), revealing that SPP1 DNA can occupy more that 35% of the cell area (Fig. 4*A*, magenta).

In order to visualize this impact of SPP1 infection on DNA spatial distribution within the cell ultrastructure, we carried out immunoelectron microscopy (immunoEM) of thin sections from *B. subtilis* YB886, an isogenic strain without fluorescent markers. DNA was localized using an anti-DNA monoclonal antibody decorated with 5 nm colloidal gold (small dots in Fig. 5 *A*, *B*, *E*, and *F*) or DNase treatment (Fig. 5 *C* and *D*) (35). In noninfected cells, two separated, symmetrically positioned bacterial nucleoids were readily observable (Fig. 5 *A*, *C*, and *E*), consistent with DAPI fluorescence staining (Fig. 5*G*). SPP1*lacO64gp2*$^{-}$ infection led to a major reorganization of the cytoplasmic space where DNA occupied a much larger region (Fig. 5*D*). The loss of the bacterial nucleoids typical position and organization in the cell (Fig. 5 *B*, *D*, *F*, and *H*) correlated with the repositioning of *B. subtilis* chromosome origins away from the viral DNA compartment (*SI Appendix*, Fig. S1*E*).

Membrane staining shows that no membrane separates the SPP1 DNA compartment from the cytoplasm (*SI Appendix*, Fig. S2*B*) (15). The unpackaged ∼125 genome copies (5.3 Mbp) of SPP1*lacO64* DNA late p.i. (Fig. 1*B*) occupy no more than ∼25% of the cytoplasm open space area (Fig. 4*A*). To investigate if the integrity of this viral DNA compartment requires active DNA replication and is energy dependent, we arrested DNA polymerase III activity with 6-(*p*-Hydroxyphenylazo)-Uracil (HPUra) (15, 36) and collapsed the proton motive force with 2,4-dinitrophenol (DNP) (37), respectively. Both HPUra and DNP prevented the formation of the viral DNA compartment at the beginning of infection. When the drugs were added after the appearance of the SPP1 DNA focus, they did not disrupt its morphological integrity (Fig. 3 *C* and *D*; SPP1 DNA panels). In HPUra-treated cells, proteins of the hybrid viral–bacterial replisome (visualized by gp40 and DnaX) lost, however, their typical pattern of discrete small foci within the DNA compartment and relocalized all over the SPP1 DNA (Fig. 3*C*). We concluded that the maintenance of SPP1 replication factories, but not of the viral DNA compartment, required active DNA synthesis. In DNP-treated cells, DnaX lost most of its association with the compartment and displayed a patchy pattern in the cytoplasm, while gp40 maintained its colocalization with SPP1 DNA (Fig. 3*D*). Thus, energy depletion leads to hybrid replisome disassembly and the dissociation of DnaX, but not of gp40, from the viral DNA compartment.

A Subpopulation of SPP1 Procapsids Localizes at the Edges of the Viral DNA Compartment. The goal of viral genome replication is to provide a nucleic acid substrate suitable for viral particles construction. In tailed bacteriophages, as in numerous viruses, replicated DNA is packaged into procapsids that are virion precursors

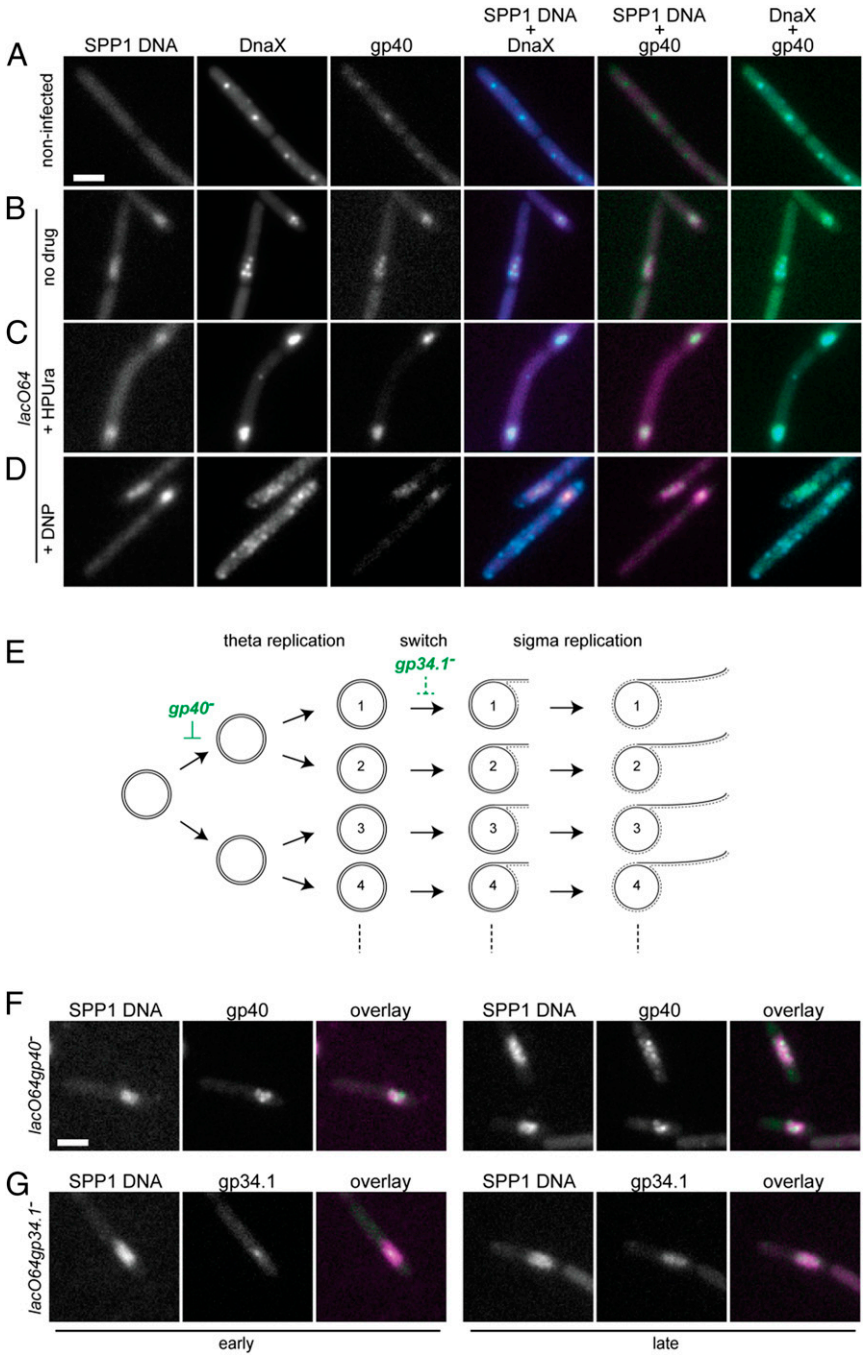

Fig. 3. Cellular localization of SPP1 proteins engaged in phage DNA replication (gp40 helicase) and in the switch of genome replication mode (gp34.1 5′-3′ exonuclease). (*A–D*) Localization of SPP1 DNA, mCFP-DnaX (*B. subtilis* clamp loader subunit), and gp40-mCitrine in noninfected bacteria (*A*) and in SPP1*lacO64*-infected bacteria untreated (*B*), incubated with 200 μM HPUra (*C*), or with 10 mM DNP (*D*). Drugs were added at 21 min p.i. to the infected culture that was spotted in an agarose pad containing the same concentration of drug 3 min later. Fluorescence microscopy acquisitions were made between 50 and 60 min p.i. (Scale bar in *A*, 2 μm.) (*E*) Scheme of SPP1 replication initiated by a theta mode, leading to an exponential increase of independent circular genome molecules followed by a switch to sigma replication that generates linear concatemers for DNA packaging. SPP1 mutants blocking replication initiation (*gp40*$^{-}$) or severely affecting the switch from theta-to-sigma mode (*gp34.1*$^{-}$) are displayed in green. (*F* and *G*) Colocalization of gp40-mCitrine (*F*) and gp34.1-mCitrine (*G*) with phage DNA in infections with SPP1 mutants defective in gp40 and in gp34.1 production (transcomplementation conditions), respectively. Images at early (*Left*) and late (*Right*) stages of infection (*SI Appendix*, Fig. S2*B*) are displayed. (Scale bar in *F*, 2 μm.)

without DNA (Fig. 5*K*), prompting investigation of their position relative to DNA in the cell. Procapsids accumulate in the cytoplasm of bacteria infected with SPP1 mutants defective for genome packaging like SPP1*lacO64gp2*$^{-}$ (18). Reliable imaging of individual phage procapsids and virions by electron microscopy (EM) of infected bacteria was hampered by sample fixation, despite extensive optimization work. However, immunolabeling of thin sections with anti-(pro)capsid antibodies showed that those structures (thick dots in Fig. 5 *B*, *D*, and *F*) accumulate at the periphery of DNA (thin dots in Fig. 5 *B* and *F*) in *B. subtilis* YB886 cells infected with SPP1*lacO64gp2*$^{-}$. Procapsid labeling was reproducibly enhanced by the digestion of DNA (Fig. 5*D*) and of

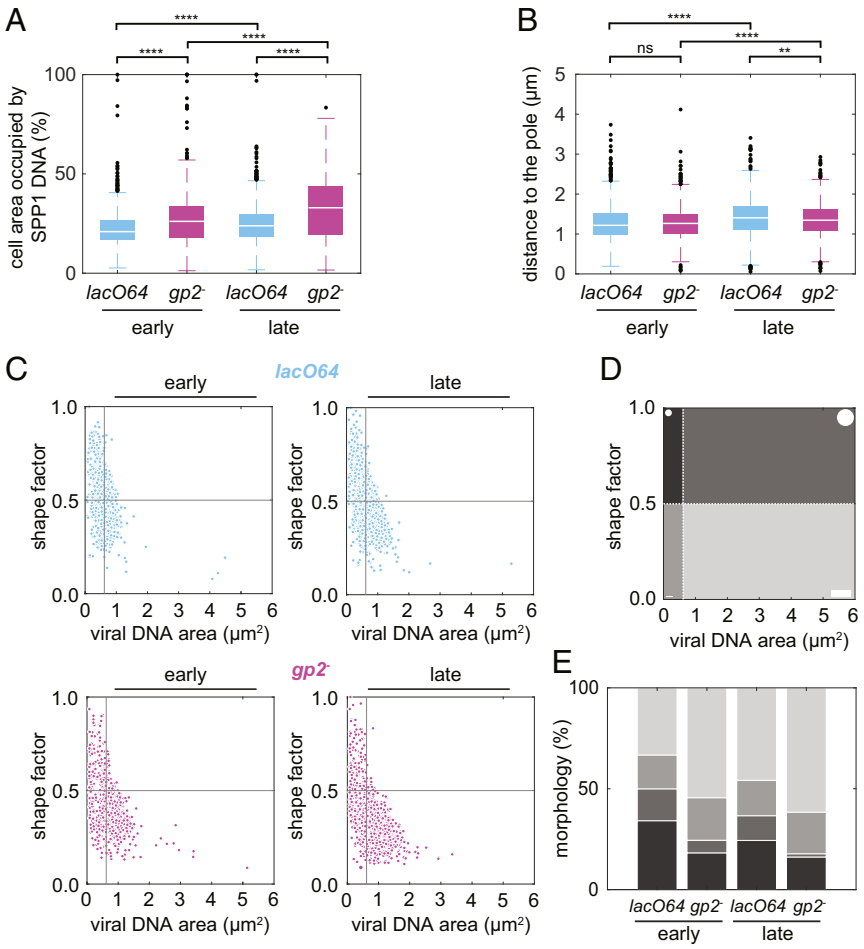

Fig. 4. Temporal evolution of the viral DNA compartment. (*A*) Percentage of cell area occupied by the SPP1 DNA focus in *B. subtilis* GSY10025 monoinfected (one viral DNA focus per cell) with SPP1*lacO64* (blue) or with the DNA packaging-defective mutant SPP1*lacO64gp2*$^{-}$ (magenta) at early and late times p.i. (*SI Appendix*, Fig. S2*B*). More than 800 cells from three independent infections were analyzed. The same datasets were used for all analyses in the figure. (*B*) Average distance of the SPP1 DNA focus center of mass to the proximal cell pole. Boxplots in *A* and *B* show the median of the sample data as a white solid line and draws point as outliers if they are greater than $q_3 + w(q_3 - q_1)$ or less than $q_1 - w(q_3 - q_1)$ in which q_1 and q_3 are the 25th and 75th percentiles of the sample data, respectively, and $w = 1.5$. Statistical significance between conditions in *A* and in *B* were calculated using the Mann–Whitney *U* nonparametric test (****$P < 0.0001$; ** $= 0.001 < P < 0.01$; * $= 0.01 < P < 0.05$; ns $= P > 0.05$). (*C*) Surface aspect of the phage DNA focus. The width-to-length ratio (shape factor) of the segmented focus is plotted relative to its area. The vertical and horizontal limits separating all quadrants are defined, respectively, as the median values of the DNA surface and the shape factor from the dataset associated with the infection with SPP1*lacO64*. Foci shape factors were quantified when DNA encapsidation took place (blue; infection with SPP1*lacO64*, abbreviated *lacO64* in the figure) or was blocked (magenta; infection with SPP1*lacO64gp2*$^{-}$, abbreviated *gp2*$^{-}$ in the figure) at early (*Left*) and late (*Right*) times p.i. (*D*) Schematic visual aid of the DNA focus shape (shape cartoon in white) observed in each quadrant of the plot in *C*. (*E*) Percentage of viral DNA compartment shape types in the quadrants of *C* displayed according to the gray scale of *D*.

trypsin-sensitive nonassembled proteins (Fig. 5*F*) in the thin sections.

We then imaged specifically SPP1 DNA with LacI-mCherry, and the procapsid scaffolding protein gp11 fused to mCitrine in live cells. Gp11 is a rod-like internal chaperone that scaffolds multimerization of the major capsid protein gp13 to build functional procapsids (38). Gp11 then exits the procapsid through holes of ~3 × 2.2 nm in the gp13 protein lattice to leave space for DNA packing (Fig. 5*K*) (39). The infection of cells producing mCitrine-gp11 with phages coding for gp11 but defective in DNA packaging (e.g., SPP1*lacO64gp2*$^{-}$ in Fig. 5*K*) led to an accumulation of procapsids in the bacterium. Their sedimentation behavior and shape were similar to SPP1 wild-type procapsids, although they carry the two gp11 forms (*SI Appendix*, Fig. S3 *A* and *B*), showing that mCitrine-gp11 is incorporated into correctly shaped procapsids during assembly. Unexpectedly, CsCl-purified phage particles produced during infection with SPP1*lacO64* contained mCitrine but not the full-length mCitrine-gp11 fusion (*SI Appendix*, Fig. S3*C*). We posited that the mCitrine β-barrel dimensions [~3 × 4 nm size in case of mCitrine (40)] precluded exit of mCitrine-gp11 through the procapsid holes and interpreted that the fusion protein was proteolyzed when its gp11 moiety left the procapsid prior to DNA packaging, leaving mCitrine stuck inside. Collectively, the data show that mCitrine-gp11 is incorporated into procapsids and that mCitrine remains inside functional structures during their subsequent maturation steps until the end of viral particle assembly.

MCitrine-gp11 distributed homogeneously in the cytoplasm of either noninfected cells (Fig. 5*I*) or cells infected with SPP1*lacO64gp13*$^{-}$ (*SI Appendix*, Fig. S3*D*), a mutant defective in the major capsid protein gp13 that does not build procapsids (Fig. 5*K*). When the procapsids assembled during infection, mCitrine-gp11 formed foci in the cell consistent with its incorporation in viral structures. In absence of DNA packaging, these foci accumulated at the phage DNA compartment periphery (Fig. 5*J* and *SI Appendix*, Fig. S3 *E* and *F*) as found in immunoEM experiments

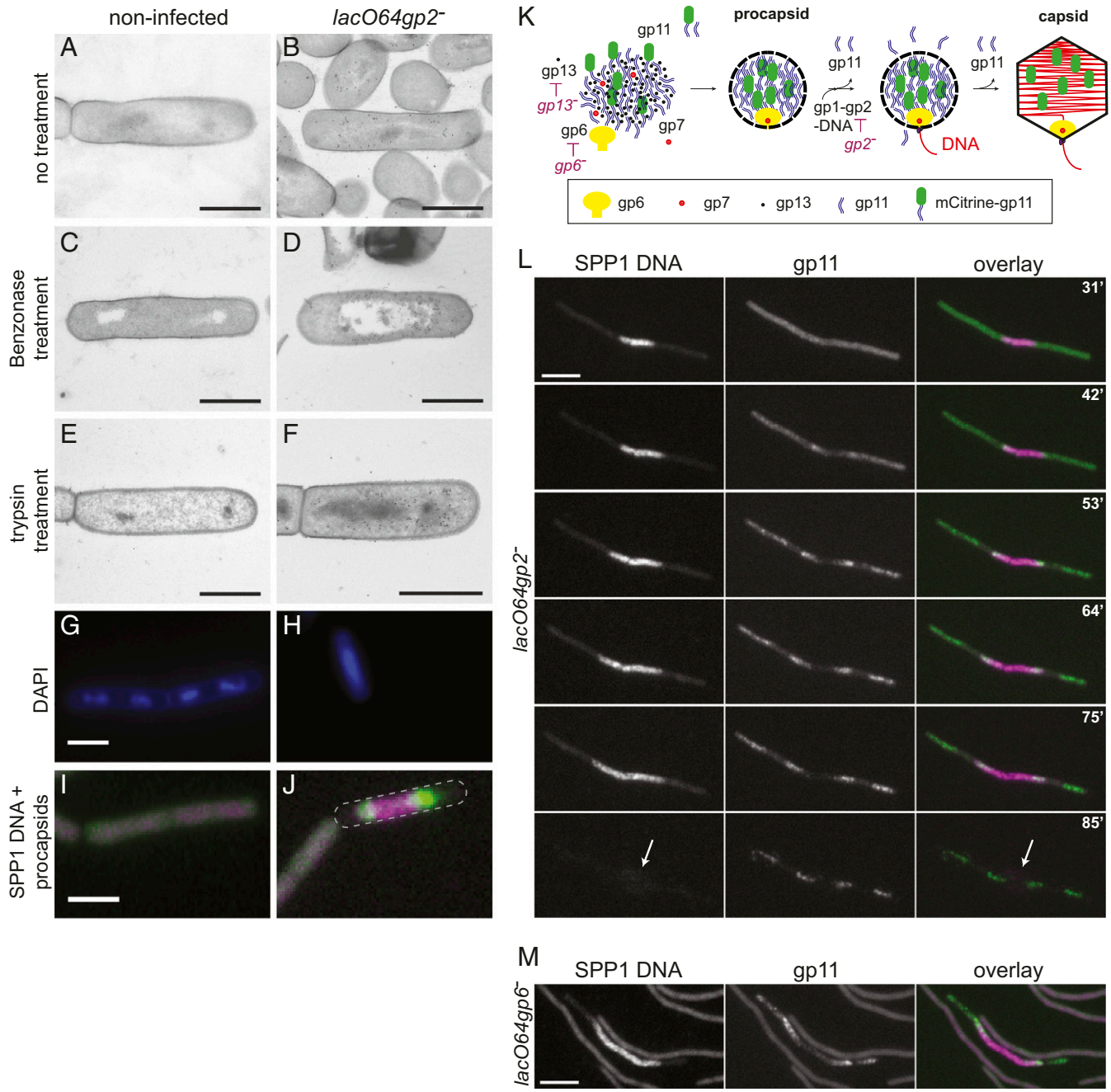

Fig. 5. Localization of SPP1 DNA and viral procapsids in infected bacteria. (*A–F*) Ultrastructure of *B. subtilis* YB886 noninfected and infected with SPP1*lacO64gp2*⁻. Sections 90-nm thick of bacteria, fixed 35 min p.i., and sectioned at cryogenic temperatures were left untreated (*A* and *B*), incubated with 25 U Benzonase (digests DNA) (*C* and *D*), or treated with 10 μg/mL trypsin [hydrolyses proteins but phage particles are resistant (43)] (*E* and *F*). Sections were labeled with a mouse monoclonal anti-DNA antibody and a rabbit polyclonal anti-procapsid serum visualized with 5 and 15 nm colloidal gold, respectively. (Scale bars in the EM sections, 1 μm.) High-resolution images of the electron micrographs in *A–F* can be found in *SI Appendix*. (*G* and *H*) Epifluorescence of fixed bacteria stained with DAPI from the cultures used for immunoEM experiments. (*I* and *J*) Cytological localization of LacI-mCherry that decorates SPP1 DNA (magenta in *J*) and of mCitrine-gp11 that is incorporated in procapsids (green in *J*) in *B. subtilis* GSY10025 noninfected and infected with SPP1*lacO64gp2*⁻. Gray dotted lines display the cell outline defined from brightfield imaging. (The scale bars represent 2 μm in the fluorescence microscopy images of *G* and *I*.) (*K*) Scheme of procapsid formation and DNA packaging initiation steps during SPP1 viral particle assembly. All components of the SPP1 procapsid and of the DNA packaging apparatus are presented. The major capsid protein gp13 lattice is displayed as a dashed line delimiting the procapsid and by a thin icosahedral outline in the expanded capsid. MCitrine is displayed as a green cylinder in the mCitrine-gp11 fusion protein. Mutants used in this study that block synthesis of different SPP1 proteins engaged in procapsid assembly and DNA packaging are also presented. (*L*) Time-lapse of filamented *B. subtilis* GSY10025 (producing mCitrine-gp11) infected with SPP1*lacO64gp2*⁻. Cell division was inhibited 1 h before infection by the addition of 1 μg/mL PC190723. Signals on the RFP and YFP channels are displayed in magenta and green in overlays, respectively. Time p.i. is displayed on the right top corner of the overlay. The arrow shows dispersion of SPP1 DNA (magenta) in the agarose pad upon cell disruption at 85 min p.i. while clusters of procapsids (green) maintain their integrity. (Scale bar, 5 μm.) (*M*) Infection of filamented *B. subtilis* GSY10025 with SPP1*lacO64gp6*⁻ defective in production of the procapsid portal protein. Portal-less procapsids assembled during infection are not competent to package viral DNA (42). An infected cell late p.i. is presented surrounded by noninfected bacteria. Experimental conditions are as in *L*.

(Fig. 5 *B*, *D*, and *F*). To follow the localization of procapsids during infection without the space constraints imposed by the cells small size, we performed time-lapse observation of mCitrine-gp11 in filamentous *B. subtilis* bacteria infected by SPP1*lacO64gp2*$^{-}$. Septation was inhibited by adding the FtsZ-inhibitor PC190723 to exponentially growing cells prior to infection, leading to the formation of long, aseptated filaments (41). The SPP1 DNA compartment became several-micrometer long in the filamentous cells before procapsids progressively accumulated at the compartment edges as well as at SPP1 DNA–free regions near the cell poles (Fig. 5*L*). Procapsids lacking the portal protein gp6 (42) showed a similar distribution (Fig. 5*M*). Interestingly, the bacterium-lysed procapsids maintained their cluster organization in the agarose pad gel used to immobilize the cells, while the SPP1 DNA compartment lost its organization (Fig. 5 *L*, *Bottom* arrow).

The localization pattern of mCitrine-gp11 had some distinctive features in cells infected by SPP1*lacO64* in which the assembly pathway of viral particles is complete. Fluorescent foci that flank the SPP1 DNA compartment are significantly better individualized and separated from the DNA compartment (*SI Appendix*, Fig. S3*G*) than those observed when only procapsids accumulate in the infected cell (*SI Appendix*, Fig. S3 *E* and *F*). Since the FP reports the localization of both procapsids and DNA-filled capsids (see above in this section), its assignment to the distribution of specific viral structures in the cell was not made.

SPP1 DNA-Filled Particles Accumulate in Spatially Independent Compartments. In order to image SPP1 capsids specifically at the post-DNA packaging state, we fused mCitrine to the nonessential capsid accessory protein gp12 (Fig. 6*A*). The binding sites of gp12 in the gp13 capsid lattice are generated during DNA encapsidation (39, 43). Consistently, when *B. subtilis* cells expressing gp12-mCitrine were infected with a DNA packaging-defective mutant, gp12 displayed a diffuse localization in the cytoplasm (Fig. 6*B*). During productive infections, gp12-mCitrine bound to DNA-filled viral particles and localized to foci flanking the phage DNA compartment both in the absence (Fig. 6*C*) and in the presence (Fig. 6*D*) of phage-encoded gp12. This spatial distribution correlated with the presence of two electrondense regions near the poles of infected cells in immunoEM thin sections that were labeled with anti-DNA and anti-capsid antibodies (Fig. 6 *E* and *G*). Infections for EM and DAPI DNA-labeling experiments (Fig. 6 *E–H*) were carried out in an isogenic strain producing no FPs to exclude the possibility that reporter fusion proteins affect the formation or properties of foci containing DNA-filled capsids. Therefore, the formation of such foci and their stronger prominence in the absence of gp12 are inherent features of SPP1 viral particles at the post-DNA packaging state (compare Figs. 5 *A*, *B*, *G*, and *H* to 6 *E–H*). In thin sections, those particles were almost certainly sectioned during preparation, rendering their DNA accessible to labeling (Fig. 6 *E* and *G*). The less compact DNA present at more central regions of the cell corresponds presumably to both SPP1 and host nonpackaged DNA (Fig. 6 *E* and *G*).

We then made triple-labeling experiments to follow the spatial distribution of capsids in the cell during their maturation from the DNA packaging step to the formation of mature virions after the addition of the tail (Fig. 6*A*). Capsids were labeled with gp12-mCFP and tails with the major tail protein gp17.1 (44) fused to mCitrine in filamented cells infected with SPP1 mutants impairing different assembly steps of the viral particle (Fig. 6*A* and *SI Appendix*, Fig. S4). When DNA packaging was arrested, gp12-mCFP remained homogenous in the bacterial cytoplasm, while foci of gp17.1-mCitrine flanked the SPP1 DNA compartment (*SI Appendix*, Fig. S4*A*). These foci, which were absent in the infection with a SPP1 mutant defective in tail formation (*SI Appendix*, Fig. S4*B*), reveal regions of tail structures clustering. During infection with SPP1*lacO64gp16*$^{-}$, the post-DNA packaging step that leads to the formation of the capsid connector interface necessary for tail binding is disrupted (45). In such situations, both capsids (gp12-mCFP label) and tails (gp17.1-mCitrine label) formed foci outside the region occupied by the SPP1 DNA compartment. Those foci were mostly spatially independent, as can be best appraised on the rightmost overlay of gp12-mCFP (blue) and gp17.1-mCitrine (yellow) signals in *SI Appendix*, Fig. S4*C*. We conclude that capsids and tails accumulate predominantly in different discrete locations within the cell when their interaction is impaired. In contrast, such segregation is not detectably observed when the assembly of tailed phage particles occurs in cells infected with SPP1*lacO64* (Fig. 6*I*). Time-lapse experiments showed that DNA-filled capsids and tails colocalize as soon as they become detectable, revealing a rapid capsid–tail association in wild-type infection conditions (*SI Appendix*, Fig. S4*D*). Therefore, the spatial distribution of SPP1 capsids and tails recapitulates precisely the post-DNA packaging sequential assembly steps (Fig. 6 *A* and *I* and *SI Appendix*, Fig. S4). We defined the compartments where mature virions are stored as warehouses.

At early infection times, the SPP1 DNA overlapped with the most proximal warehouse identified by the gp12 focus in ∼50% of the cells (Fig. 6*J*). Late in infection, most gp12-mCitrine had relocalized to positions distant from the SPP1 DNA (Fig. 6 *C*, *D*, and *J*). Automated segmentation of fluorescent gp12-mCitrine foci in monoinfected cells confirmed that there are multiple foci early in infection, which likely merge afterward to form two or three warehouses (*SI Appendix*, Fig. S5*A*). In cells containing two warehouses, these were generally found on either side of the viral DNA compartment (*SI Appendix*, Fig. S5*B*) at different relative distances (*SI Appendix*, Fig. S5 *C* and *D*). Their fluorescence intensity revealed a roughly similar distribution of DNA-filled particles between the two warehouses (*SI Appendix*, Fig. S5*E*). We next analyzed the gp12-mCitrine focus proximal to the viral DNA compartment to follow the evolution of warehouses during infection. The surface of the warehouses increased moderately during infection (*SI Appendix*, Fig. S5*F*) and they remained quasi-spherical (*SI Appendix*, Fig. S5*G*). However, their fluorescence intensity raised significantly (*SI Appendix*, Fig. S5*H*), suggesting that DNA-filled particles adopt a more compact organization in the warehouse with time. Gp12-mCitrine foci formed in the absence of phage-encoded gp12 were more compact and brighter than the ones built in the presence of phage-encoded gp12 (*SI Appendix*, Fig. S5 *F–H*).

We next visualized the complete spatiotemporal program of viral DNA compartment and virion warehouse formation during the infection of gp12-mCitrine-producing cells with SPP1*lacO64gp12*$^{-}$ in real time using a microfluidics device (Fig. 6*K* and Movie S1). Quasi-circular phage DNA compartments formed first and then elongated throughout infection until cell lysis. Flanking, spatially independent warehouses of DNA-filled particles appeared later. They grew initially to a defined circular shape and then became more intense without major change in their size. Interestingly, bacteria continued to elongate and to divide during infection (white arrow in Fig. 6*K*), although their growth in liquid medium was slightly reduced relative to noninfected bacteria (*SI Appendix*, Fig. S1*B*). In some cells, the division septum sectioned the viral DNA compartment partitioning phage genome copies between daughter cells in which SPP1 DNA continued to replicate (Fig. 6*L*).

Discussion

We have discovered that bacteriophage SPP1 infection generates compartments in the crowded bacterial cytoplasm that have neither membrane nor protein cage boundaries. The spatiotemporal independent compartments confine viral DNA transactions and storage of viral particles. This spatial partition responds to the requirements for accommodating exponential replication of the viral genome and assembly of hundreds of infectious viral particles, the two central processes of the viral lytic cycle. The resulting major quantitative perturbation is the amount of viral DNA synthesized,

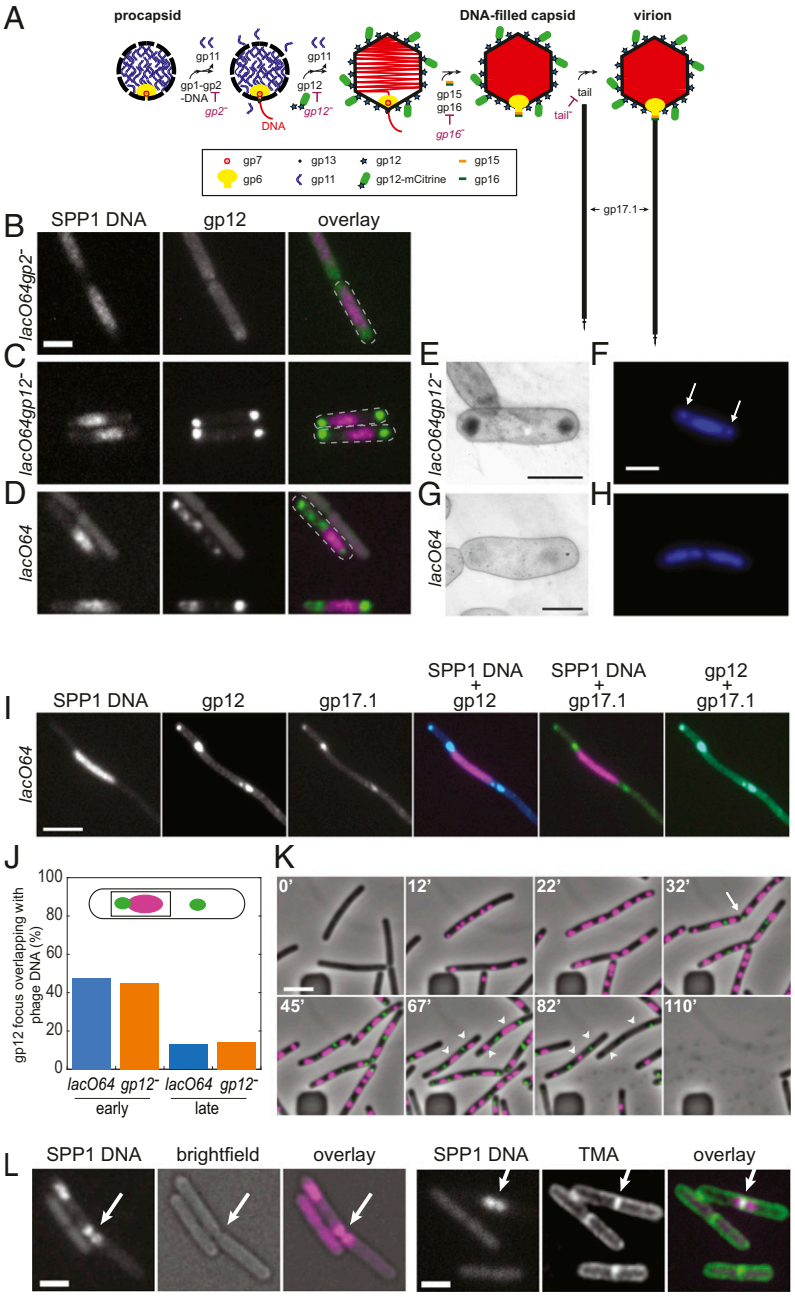

Fig. 6. Localization of SPP1 DNA and DNA-filled particles in infected bacteria. (*A*) Scheme of the SPP1 viral particle assembly pathway. MCitrine is displayed as a green cylinder in the gp12-mCitrine fusion protein. (*B–D*) Localization of SPP1 DNA and of capsid auxiliary protein gp12-mCitrine that decorates DNA-filled particles in *B. subtilis* GSY10024 infected with SPP1*lacO64gp2*$^{-}$ (*B*), SPP1*lacO64gp12*$^{-}$ (*C*), and SPP1*lacO64* (*D*). Images at late stages of infection (*SI Appendix*, Fig. S2*B*) are displayed. Gray dotted lines display cell outlines defined from brightfield imaging. (Scale bar, 2 μm.) (*E* and *G*) Thin sections of *B. subtilis* YB886 infected with SPP1*lacO64gp12*$^{-}$ (*E*) and SPP1*lacO64* (*G*) immunolabeled as in Fig. 5 *A* and *B*. (Scale bars, 1 μm.) High-resolution images of the electron micrographs in *E* and *G* can be found in *SI Appendix*. (*F* and *H*) DAPI staining of fixed bacteria from the cultures used for immunoEM experiments. Arrows in *F* identify individualized DAPI foci attributed to warehouses. (Scale bar in *F*, 2 μm.) (*I*) Infection of *B. subtilis* GSY10096-filamented cells with SPP1*lacO64*. The fluorescent reporters of SPP1 DNA, capsids, and tails were LacI-mCherry (magenta in overlays), gp12-mCFP (blue), and gp17.1-mCitrine (green), respectively. Images were taken late p.i. (Scale bar, 5 μm.) (*J*) Quantification of DNA-filled particles overlapping with the phage DNA compartment of cells monoinfected with SPP1*lacO64* and SPP1*lacO64gp12*$^{-}$ at early and late times p.i. Datasets of >500 cells were analyzed. (*K*) Snapshots from time-lapse Movie S1 of *B. subtilis* GSY10024, producing gp12-mCitrine, immobilized in a CellAsic microfluidics system and infected with SPP1*lacO64gp12*$^{-}$. The first photo shows cells before infection followed by snapshots at time points indicated on the top left corner. They illustrate the temporal and spatial program of SPP1 DNA compartment and viral particles warehouses formation (displayed in magenta and green, respectively). Cells are multi-infected. The white arrow identifies a bacterium undergoing division. The arrowheads show the position of DNA compartments at 67 min p.i. that are disassembled in cell ghosts at 82 min p.i. but prior to full bacterial lysis (110 min p.i.). Images were enhanced as described in the Movie S1 legend. (*L*) Cell septation through the SPP1 DNA compartment (displayed in magenta) in bacteria producing LacI-mCherry (strain GSY10004) infected with SPP1*lacO64*. The cell membrane contour is stained with TMA-DPH (rendered in green) on the right side. The white arrow shows septum formation. To enhance the signal from the membrane staining (TMA-DPH), the raw image was denoised (two-dimensional Gaussian filter, radius = 1, 25 pixel) and background was removed using a rolling ball (sigma = 10 pixels) using Fiji (67).

which rises greater than twofold the total cell DNA mass (Fig. 1*B* and Dataset S1). Concomitantly, bacterial nucleoids lose their regular position and condensed organization in the cell (Fig. 5 *A–H* and *SI Appendix*, Fig. S1*E*). These changes in the *B. subtilis* chromosome organization can be attributed to the arrest of its replication (46) by hijacking bacterial replisomes to replicate SPP1 DNA (Fig. 2 and *SI Appendix*, Fig. S2*C*), although some bacterial DNA synthesis still proceeds during infection (*SI Appendix*, Fig. S1*F*). The area occupied by DNA in infected bacteria increases without a detectable change on average cell size despite the mechanism that maintains a constant nucleocytoplasmic ratio across bacteria, including *B. subtilis* (47). Hence, viral DNA can occupy more than 35% of the cell area (Figs. 4*A* and 5*D*). Such spatial stress is relieved by DNA packaging, which strips off proteins bound to the viral DNA to tightly pack it in capsids at a concentration of ∼415 mg/mL, liberating space for higher yield DNA synthesis (Fig. 1*D*).

The single SPP1 DNA molecule entering the cytoplasm of monoinfected bacteria seeds the viral-induced DNA compartment found at a unique asymmetric position in the cell. This finding shows that the 44 kbp circular molecules generated by initial theta replication of the SPP1 genome (Fig. 3*E*) do not segregate to establish independent replication compartments. Rather, they stay confined together at a defined position of the cell. Similarly, eukaryotic herpesviruses, which are phylogenetically related to tailed phages (48), assemble discrete DNA replication compartments in the cell nucleus, each originating from a single incoming genome (49). Biogenesis of the viral DNA compartment can be partially explained by the accumulation of replicated SPP1 DNA at a defined position of the cytoplasm. Polymer dynamics simulations predict that long DNA molecules fold to a compact globular shape in a crowded confined space like the cellular environment (1). Further compaction is likely achieved by protein–DNA interactions (e.g., with nucleoid-associated proteins), while binding of other proteins may antagonize it to ensure the accessibility of genome sequences to DNA transactions like DNA replication, recombination, transcription, or encapsidation into viral procapsids (1, 50–52). These combined effects can explain the formation of a self-contained compartment with neither membrane nor protein cage boundaries. Its constrained metastable state is nearly instantaneously lost upon infection-induced cell lysis and death (e.g., 82 min p.i. in Fig. 6*K* and Movie S1), probably due to the reduction of cytoplasmic crowding following leakage of the cell content. We also showed that the division septum can cut through the SPP1 DNA compartment during cell division, delivering viral genomes to the two daughter cells (Fig. 6*L*). This is advantageous for the phage, rendering superfluous an occlusion mechanism similar to the one employed by bacteria to prevent the sectioning of their chromosome (53).

We found that SPP1–host hybrid replisome components colocalize at multiple discrete foci inside the viral DNA compartment. In contrast to the compartment integrity, stable maintenance of those punctuate hybrid replisome foci is DNA replication and energy dependent (Fig. 3 *B–D*). We posit that they correspond to parallelized factories synthesizing DNA from several independent templates (Fig. 3*E*), which are necessary to sustain the viral genome replication rate during infection. Considering that SPP1*lacO64* synthesizes 278 copies of its 42.3 kbp genome within 15 min (15 to 30 min p.i. in Fig. 1*B*), this corresponds to an average synthesis rate of 13.1 kbp/s. There are thus at least 13 fully operative DNA replication machines synthesizing at a rate of 1,000 base pairs/s (54) distributed at different locations within the DNA compartment ultrastructure.

The localization of procapsids at the periphery of the SPP1 DNA compartment (Fig. 5) identifies the most likely position of replicated DNA packaging reactions into procapsids. A related spatial organization was found in the nucleus of cells infected by the human Herpes Simplex Virus 1 (HSV-1), whose procapsids cluster at positions adjacent to the virus DNA replication centers (55). The presence of DNA replication and DNA packaging molecular machineries in the same compartment provides a cytological basis for their cross talk as reported for phages T4 (56) and SPP1 (57) as well as for the regulatory feedback we observed between the two processes (Fig. 1*D*). The two machineries must also work together in bacteriophages T3, T7, and T5, which require resynthesis of DNA concomitantly with genome packaging to generate terminal repetitions of identical sequence in the DNA molecules encapsidated (58). Collectively, our data rationalize previous observations in several viral systems, defining the viral-induced DNA compartment as the central industrial hub to sequester the proteins required for DNA transactions and to couple spatially their reactions in the infected cell. It also reveals a strategy to confine viral DNA processes different from the protein cage used by jumbo phages to compartmentalize their DNA at midcell (10, 11).

SPP1 capsids do not remain associated with the viral DNA compartment after DNA packaging, a morphogenetic step that is characterized by the transition from the procapsid to the DNA-filled capsid state. This transition creates the binding sites for the nonessential auxiliary protein gp12 at the capsid surface (39, 43) and the interface for tails binding to the capsid connector. The latter reaction leads to a formation of infectious virions (Fig. 6*A*). Virions accumulate in a different type of compartment, the warehouse (Fig. 6 and *SI Appendix*, Figs. S4 and S5), irrespectively of gp12 binding to capsids. Particles lacking gp12 form warehouses significantly more compact than those with gp12 do (Fig. 6 *C–H*). This finding shows that the properties of the phage icosahedral capsid surface play a main role on warehouse organization and possibly also on its biogenesis. We hypothesize that it is the smooth (59), albeit more electronegative, surface of capsids lacking gp12 (43) that facilitates their tighter association in warehouses when compared to capsids decorated with arrays of flexible, symmetrically arranged gp12 trimers (39, 59). The orderly packing of a large number of phage particles through their capsid icosahedral lattices is certainly disturbed by the presence of tail structures. Such constrain makes it unlikely to reach a crystal-like arrangement of viral particles as found for HSV-1 and polyomavirus capsids in the nucleus of infected eukaryotic cells (60, 61). The formation of phage warehouses fulfills, nevertheless, their putative function to minimize the storage space of viral particles in the cell.

The SPP1 DNA is in direct contact with the cytoplasm, rendering it vulnerable to cellular defenses like CRISPR-Cas (62) in contrast to the nucleus-like protein cage used by jumbo phages to protect their DNA (12, 63). Although this is a limitation for SPP1 exploration of host's landscape, such cost is plausibly compensated by the competitive advantage of its much higher burst size and shorter infection period when compared to jumbo phages multiplication parameters (64). A different way to exploit the cytoplasm open space is typified by bacteriophage phage ϕ29 that targets the MreB bacterial cytoskeleton to structure its DNA replication at the periphery of the cell interior (8, 9). This strategy allows for the production of a high burst of infectious virions but might be limited to the few viruses that replicate their DNA by a protein-primed replication mechanism. The SPP1 different compartments properties offer a cost- and time-effective way to exchange protein effectors between the cellular pool and viral compartments to fulfill the needs for phage multiplication. Protein enrollment follows a defined order. This principle is well illustrated by the assembly of SPP1 viral particles. Their building blocks are recruited from homogeneous cytoplasmic pools to a defined subcellular localization, following an order that recapitulates the program of viral particle sequential assembly. That is shown in our study for the scaffolding protein gp11 at the procapsid assembly stage (*SI Appendix*, Fig. S3 *D–G*), the capsid accessory protein

gp12 at the post-DNA packaging state (Fig. 6 *B–D*), and the tail fixation to the capsid connector interface (*SI Appendix*, Fig. S4).

The ways in how SPP1 restructures the infected cell are most probably used by a large number of phages. SPP1 partition of cytoplasmic space has also a number of striking similarities with the remodeling of the eukaryotic cell nucleus during infection by herpesviruses (see above in *Discussion* and refs. 49 and 55 and references therein). Those changes of cell architecture concur with common molecular mechanisms of recombination-dependent DNA replication (17) and packaging into viral procapsids (65). We propose that SPP1 typifies ancestral strategies used by viruses to organize the cellular space that were conserved to infect hosts of different domains of life.

Materials and Methods

A complete list of bacterial strains, phages, plasmids, antibodies, and primers used in this work is presented in *SI Appendix*, Table S3.

A detailed description of all the methods is provided in *SI Appendix*, *Materials and Methods* that includes bacterial, phages, and plasmids construction; phages amplification and infection studies; purification and characterization of phage particles; qPCR; fluorescence microscopy, microfluidics, and quantitative imaging of infected bacteria; electron microscopy; and statistical analyses. The MatLab scripts used in this work and a tutorial were uploaded to a repository in GitHub for open access: https://github.com/CyrilleBillaudeau/TemporalCompartmentalization_ofViral_Infection_inBactCells.

Data Availability. All study data are included in the article and/or supporting information.

ACKNOWLEDGMENTS. Part of this work is from the PhD thesis of A.L. at Université Paris-Saclay. Naima Nhiri is acknowledged for her most helpful support on qPCR and Qubit experiments. We are very thankful to Mart Krupovic for providing up-to-date quantitative information on tailed phages genome size. We acknowledge Laetitia Maroc for participation on the analysis of procapsids composition. We are also grateful to Arnaud Chastanet for advice to setup the microfluidics experiments. We thank Etienne Dervyn, Alan D Grossman, Catherine Ann Lee, Jeff Errington, Heath Murray, Ling Juan Wu, Adriano Henriques, David Rudner, Thierry Doan, Dan Zeigler, and the Bacillus Genetic Stock Center for providing strains used in this study. We are grateful to Neal Brown, George Wright, and Neal Agneta (GLSynthesis) for HPUra. Sandrine Brasilès is acknowledged for anti-SPP1 procapsids rabbit serum. We thank Arnaud Chastanet, Marta de Frutos, and Eric Cascales for fruitful discussions. Thanks also to Magali Ventroux for comments on the manuscript. We acknowledge Marta de Frutos (Laboratoire de Physique des Solides, Université Paris-Saclay, Orsay) for rendering available one of the fluorescence microscopes used in this work. This microscope was funded by the CNRS Actions interdisciplinaires, Interface physique-chimie-biologie: Soutien à la prise de risque (2011) and by the Université de Paris-Sud Appel d'offre Attractivité (2010). Microscope upgrades and acquisition of a Cellasics microfluidics was funded by Fondation pour la Recherche Médicale (FRM). L.J. was supported by the University of Vilnius, the Université Paris-Sud, the French embassy in Lithuania, the program Egide Gilibert between France and Lithuania, the European Union Erasmus Program, and the Région Ile-de-France. This work was funded by grants from FRM (to P.T.), Agence Nationale de la Recherche (ANR) BacVirFactory and BacVirRemodel (to P.T. and R.C.-L.), Ministerio de Economía y Competitividad (MINECO) and Ministerio de Ciencias y Universidades (MCIU) (to S.A.), and institutional funding from CNRS (P.T.), Institut National de Recherche pour l'Agriculture, l'Alimentation et l'Environnement (INRAE) (R.C.-L.), and Max-Planck-Institut for Molecular Genetics (MPIMG) (T.M.).

1. I. V. Surovtsev, C. Jacobs-Wagner, Subcellular organization: A critical feature of bacterial cell replication. *Cell* **172**, 1271–1293 (2018).
2. E. Cornejo, N. Abreu, A. Komeili, Compartmentalization and organelle formation in bacteria. *Curr. Opin. Cell Biol.* **26**, 132–138 (2014).
3. C. V. Iancu *et al*., Organization, structure, and assembly of α-carboxysomes determined by electron cryotomography of intact cells. *J. Mol. Biol.* **396**, 105–117 (2010).
4. C. A. McHugh *et al*., A virus capsid-like nanocompartment that stores iron and protects bacteria from oxidative stress. *EMBO J.* **33**, 1896–1911 (2014).
5. M. Schmid, T. Speiseder, T. Dobner, R. A. Gonzalez, DNA virus replication compartments. *J. Virol.* **88**, 1404–1420 (2014).
6. C. Risco *et al*., Three-dimensional imaging of viral infections. *Annu. Rev. Virol.* **1**, 453–473 (2014).
7. J. Nikolic *et al*., Negri bodies are viral factories with properties of liquid organelles. *Nat. Commun.* **8**, 58 (2017).
8. D. Muñoz-Espín *et al*., The actin-like MreB cytoskeleton organizes viral DNA replication in bacteria. *Proc. Natl. Acad. Sci. U.S.A.* **106**, 13347–13352 (2009).
9. D. Muñoz-Espín, I. Holguera, D. Ballesteros-Plaza, R. Carballido-López, M. Salas, Viral terminal protein directs early organization of phage DNA replication at the bacterial nucleoid. *Proc. Natl. Acad. Sci. U.S.A.* **107**, 16548–16553 (2010).
10. V. Chaikeeratisak *et al*., Assembly of a nucleus-like structure during viral replication in bacteria. *Science* **355**, 194–197 (2017).
11. V. Chaikeeratisak *et al*., Viral capsid trafficking along treadmilling tubulin filaments in bacteria. *Cell* **177**, 1771–1780.e12 (2019).
12. L. M. Malone *et al*., A jumbo phage that forms a nucleus-like structure evades CRISPR-Cas DNA targeting but is vulnerable to type III RNA-based immunity. *Nat. Microbiol.* **5**, 48–55 (2020).
13. M. Krupovic, V. Cvirkaite-Krupovic, J. Iranzo, D. Prangishvili, E. V. Koonin, Viruses of archaea: Structural, functional, environmental and evolutionary genomics. *Virus Res.* **244**, 181–193 (2018).
14. R. Edgar *et al*., Bacteriophage infection is targeted to cellular poles. *Mol. Microbiol.* **68**, 1107–1116 (2008).
15. L. Jakutytė *et al*., Bacteriophage infection in rod-shaped gram-positive bacteria: Evidence for a preferential polar route for phage SPP1 entry in Bacillus subtilis. *J. Bacteriol.* **193**, 4893–4903 (2011).
16. J. C. Alonso, P. Tavares, R. Lurz, T. A. Trautner, "Bacteriophage SPP1" in *The Bacteriophages*, R. Calendar, Ed. (Oxford University Press, New York, NY, ed. 2, 2006), pp. 331–349.
17. A. Lo Piano, M. I. Martínez-Jiménez, L. Zecchi, S. Ayora, Recombination-dependent concatemeric viral DNA replication. *Virus Res.* **160**, 1–14 (2011).
18. L. Oliveira, P. Tavares, J. C. Alonso, Headful DNA packaging: Bacteriophage SPP1 as a model system. *Virus Res.* **173**, 247–259 (2013).
19. E. Tzipilevich, M. Habusha, S. Ben-Yehuda, Acquisition of phage sensitivity by bacteria through exchange of phage receptors. *Cell* **168**, 186–199.e12 (2017).
20. L. M. Godinho *et al*., The revisited genome of Bacillus subtilis bacteriophage SPP1. *Viruses* **10**, 1–28 (2018).
21. H. Murray, J. Errington, Dynamic control of the DNA replication initiation protein DnaA by Soj/ParA. *Cell* **135**, 74–84 (2008).
22. P. Tavares, The Bacteriophage head-to-tail interface. *Subcell. Biochem.* **88**, 305–328 (2018).
23. S. Chai *et al*., Molecular analysis of the Bacillus subtilis bacteriophage SPP1 region encompassing genes 1 to 6. The products of gene 1 and gene 2 are required for pac cleavage. *J. Mol. Biol.* **224**, 87–102 (1992).
24. X. Pedré, F. Weise, S. Chai, G. Lüder, J. C. Alonso, Analysis of cis and trans acting elements required for the initiation of DNA replication in the Bacillus subtilis bacteriophage SPP1. *J. Mol. Biol.* **236**, 1324–1340 (1994).
25. E. M. Seco *et al*., Bacteriophage SPP1 DNA replication strategies promote viral and disable host replication in vitro. *Nucleic Acids Res.* **41**, 1711–1721 (2013).
26. E. M. Seco, S. Ayora, Bacillus subtilis DNA polymerases, PolC and DnaE, are required for both leading and lagging strand synthesis in SPP1 origin-dependent DNA replication. *Nucleic Acids Res.* **45**, 8302–8313 (2017).
27. J. C. Meile, L. J. Wu, S. D. Ehrlich, J. Errington, P. Noirot, Systematic localisation of proteins fused to the green fluorescent protein in Bacillus subtilis: Identification of new proteins at the DNA replication factory. *Proteomics* **6**, 2135–2146 (2006).
28. E. Dervyn *et al*., Two essential DNA polymerases at the bacterial replication fork. *Science* **294**, 1716–1719 (2001).
29. R. Missich *et al*., The replisome organizer (G38P) of Bacillus subtilis bacteriophage SPP1 forms specialized nucleoprotein complexes with two discrete distant regions of the SPP1 genome. *J. Mol. Biol.* **270**, 50–64 (1997).
30. S. Ayora, A. Stasiak, J. C. Alonso, The Bacillus subtilis bacteriophage SPP1 G39P delivers and activates the G40P DNA helicase upon interacting with the G38P-bound replication origin. *J. Mol. Biol.* **288**, 71–85 (1999).
31. M. I. Martínez-Jiménez, P. Mesa, J. C. Alonso, Bacillus subtilis τ subunit of DNA polymerase III interacts with bacteriophage SPP1 replicative DNA helicase G40P. *Nucleic Acids Res.* **30**, 5056–5064 (2002).
32. S. Ayora, U. Langer, J. C. Alonso, Bacillus subtilis DnaG primase stabilises the bacteriophage SPP1 G40P helicase-ssDNA complex. *FEBS Lett.* **439**, 59–62 (1998).
33. G. Wang *et al*., The structure of a DnaB-family replicative helicase and its interactions with primase. *Nat. Struct. Mol. Biol.* **15**, 94–100 (2008).
34. A. Valero-Rello, M. López-Sanz, A. Quevedo-Olmos, A. Sorokin, S. Ayora, Molecular mechanisms that contribute to horizontal transfer of plasmids by the bacteriophage SPP1. *Front. Microbiol.* **8**, 1816 (2017).
35. B. Bohrmann, E. Kellenberger, Immunostaining of DNA in electron microscopy: An amplification and staining procedure for thin sections as alternative to gold labeling. *J. Histochem. Cytochem.* **42**, 635–643 (1994).
36. S. D. Rowley, N. C. Brown, Bacillus subtilis DNA polymerase III is required for the replication of DNA of bacteriophages SPP-1 and ϕ 105. *J. Virol.* **21**, 493–496 (1977).
37. A. Lamsa, W.-T. Liu, P. C. Dorrestein, K. Pogliano, The Bacillus subtilis cannibalism toxin SDP collapses the proton motive force and induces autolysis. *Mol. Microbiol.* **84**, 486–500 (2012).
38. S. L. Poh *et al*., Oligomerization of the SPP1 scaffolding protein. *J. Mol. Biol.* **378**, 551–564 (2008).
39. A. Ignatiou *et al*., Structural transitions during the scaffolding-driven assembly of a viral capsid. *Nat. Commun.* **10**, 4840 (2019).
40. O. Griesbeck, G. S. Baird, R. E. Campbell, D. A. Zacharias, R. Y. Tsien, Reducing the environmental sensitivity of yellow fluorescent protein. Mechanism and applications. *J. Biol. Chem.* **276**, 29188–29194 (2001).
41. D. J. Haydon *et al*., An inhibitor of FtsZ with potent and selective anti-staphylococcal activity. *Science* **321**, 1673–1675 (2008).

42. A. Dröge *et al*., Shape and DNA packaging activity of bacteriophage SPP1 procapsid: Protein components and interactions during assembly. *J. Mol. Biol.* **296**, 117–132 (2000).
43. M. Zairi, A. C. Stiege, N. Nhiri, E. Jacquet, P. Tavares, The collagen-like protein gp12 is a temperature-dependent reversible binder of SPP1 viral capsids. *J. Biol. Chem.* **289**, 27169–27181 (2014).
44. I. Auzat, A. Dröge, F. Weise, R. Lurz, P. Tavares, Origin and function of the two major tail proteins of bacteriophage SPP1. *Mol. Microbiol.* **70**, 557–569 (2008).
45. E. V. Orlova *et al*., Structure of a viral DNA gatekeeper at 10 A resolution by cryo-electron microscopy. *EMBO J.* **22**, 1255–1262 (2003).
46. M. Marbouty *et al*., Condensin- and replication-mediated bacterial chromosome folding and origin condensation revealed by Hi-C and Super-resolution imaging. *Mol. Cell* **59**, 588–602 (2015).
47. W. T. Gray *et al*., Nucleoid size scaling and intracellular organization of translation across bacteria. *Cell* **177**, 1632–1648.e20 (2019).
48. J. Iranzo, M. Krupovic, E. V. Koonin, The double-stranded DNA virosphere as a modular hierarchical network of gene sharing. *mBio* **7**, 1–21 (2016).
49. O. Kobiler, P. Brodersen, M. P. Taylor, E. B. Ludmir, L. W. Enquist, Herpesvirus replication compartments originate with single incoming viral genomes. *mBio* **2**, 1–9 (2011).
50. J. K. Fisher *et al*., Four-dimensional imaging of E. coli nucleoid organization and dynamics in living cells. *Cell* **153**, 882–895 (2013).
51. S. Cunha, C. L. Woldringh, T. Odijk, Polymer-mediated compaction and internal dynamics of isolated Escherichia coli nucleoids. *J. Struct. Biol.* **136**, 53–66 (2001).
52. S. C. Verma, Z. Qian, S. L. Adhya, Architecture of the Escherichia coli nucleoid. *PLoS Genet.* **15**, e1008456 (2019).
53. D. W. Adams, L. J. Wu, J. Errington, Cell cycle regulation by the bacterial nucleoid. *Curr. Opin. Microbiol.* **22**, 94–101 (2014).
54. M. O'Donnell, L. Langston, B. Stillman, Principles and concepts of DNA replication in bacteria, archaea, and eukarya. *Cold Spring Harb. Perspect. Biol.* **5**, 1–14 (2013).
55. P. L. Ward, W. O. Ogle, B. Roizman, Assemblons: Nuclear structures defined by aggregation of immature capsids and some tegument proteins of herpes simplex virus 1. *J. Virol.* **70**, 4623–4631 (1996).
56. V. B. Rao, L. W. Black, "DNA packaging in bacteriophage T4" in *Viral Genome Packaging Machines: Genetics, Structure, and Mechanism*, C. E. Catalano, Ed. (Plenum Press, 2005), pp. 40–58.
57. P. Tavares, R. Lurz, A. Stiege, B. Rückert, T. A. Trautner, Sequential headful packaging and fate of the cleaved DNA ends in bacteriophage SPP1. *J. Mol. Biol.* **264**, 954–967 (1996).
58. L. W. Black, DNA packaging in dsDNA bacteriophages. *Annu. Rev. Microbiol.* **43**, 267–292 (1989).
59. H. E. White *et al*., Capsid structure and its stability at the late stages of bacteriophage SPP1 assembly. *J. Virol.* **86**, 6768–6777 (2012).
60. K. Miyamoto, Mechanism of intranuclear crystal formation of herpes simplex virus as revealed by the negative staining of thin sections. *J. Virol.* **8**, 534–550 (1971).
61. K. D. Erickson *et al*., Virion assembly factories in the nucleus of polyomavirus-infected cells. *PLoS Pathog.* **8**, e1002630 (2012).
62. L. Jakutyte-Giraitiene, G. Gasiunas, Design of a CRISPR-Cas system to increase resistance of Bacillus subtilis to bacteriophage SPP1. *J. Ind. Microbiol. Biotechnol.* **43**, 1183–1188 (2016).
63. S. D. Mendoza *et al*., A bacteriophage nucleus-like compartment shields DNA from CRISPR nucleases. *Nature* **577**, 244–248 (2020).
64. J. A. Kraemer *et al*., A phage tubulin assembles dynamic filaments by an atypical mechanism to center viral DNA within the host cell. *Cell* **149**, 1488–1499 (2012).
65. F. J. Rixon, M. F. Schmid, Structural similarities in DNA packaging and delivery apparatuses in Herpesvirus and dsDNA bacteriophages. *Curr. Opin. Virol.* **5**, 105–110 (2014).
66. C. São-José, M. de Frutos, E. Raspaud, M. A. Santos, P. Tavares, Pressure built by DNA packing inside virions: Enough to drive DNA ejection in vitro, largely insufficient for delivery into the bacterial cytoplasm. *J. Mol. Biol.* **374**, 346–355 (2007).
67. J. Schindelin *et al*., Fiji: An open-source platform for biological-image analysis. *Nat. Methods* **9**, 676–682 (2012).